Journal of Sound and Vibration 329 (2010) 4440–4454

Contents lists available at ScienceDirect

Journal of Sound and Vibration

journal homepage: www.elsevier.com/locate/jsvi

Symplectic random vibration analysis of a vehicle moving on an infinitely long periodic track

You-Wei Zhang [a], Jia-Hao Lin [a], Yan Zhao [a,*], W.P. Howson [b], F.W. Williams [b]

[a] State Key Laboratory of Structural Analysis for Industrial Equipment, Faculty of Vehicle Engineering and Mechanics, Dalian University of Technology, Dalian 116023, PR China

[b] Cardiff School of Engineering, Cardiff University, Cardiff CF24 3AA, Wales, UK

ARTICLE INFO

Article history:
Received 19 November 2009
Received in revised form
31 March 2010
Accepted 6 May 2010
Handling Editor: H. Ouyang
Available online 8 June 2010

ABSTRACT

Based on the pseudo-excitation method (PEM), symplectic mathematical scheme and Schur decomposition, the random responses of coupled vehicle–track systems are analyzed. The vehicle is modeled as a spring–mass–damper system and the track is regarded as an infinitely long substructural chain consisting of three layers, i.e. the rails, sleepers and ballast. The vehicle and track are coupled via linear springs and the "moving-vehicle model" is adopted. The latter assumes that the vehicle moves along a static track for which the rail irregularity is further assumed to be a zero-mean valued stationary Gaussian random process. The problem is then solved efficiently as follows. Initially, PEM is used to transform the rail random excitations into deterministic harmonic excitations. The symplectic mathematical scheme is then applied to establish a low degree of freedom equation of motion with periodic coefficients. In turn these are transformed into a linear equation set whose upper triangular coefficient matrix is established using the Schur decomposition scheme. Finally, the frequency-dependent terms are separated from the load vector to avoid repeated computations for different frequencies associated with the pseudo-excitations. The proposed method is subsequently justified by comparison with a Monte-Carlo simulation; the fixed-vehicle model and the moving-vehicle model are compared and the influences of vehicle velocity and class of track on system responses are also discussed.

1. Introduction

When a vehicle moves along a track, the track irregularity is a very important source of random excitation, so that analysis of the coupled system subjected to such excitation is of great importance for vehicle/track design and maintenance.

Very few studies have concentrated on the random vibration analysis of a coupled vehicle–track system. Usually, two kinds of excitation model are considered: the fixed-vehicle model and the moving-vehicle model. The former assumes that the vehicle remains stationary relative to the track and that the track irregularities move backwards at the velocity of the vehicle. This model can be used easily in a frequency domain analysis. It was used by Chen [1] and Li and Wan [2] to derive the response power spectral densities (PSDs) and Lu et al. [3] who regarded the track as an infinitely long substructural chain in order to develop a very efficient method for analysing the random responses using the pseudo-excitation method (PEM) and the symplectic mathematical scheme. Xu et al. [4] investigated the vertical random vibration of the track

* Corresponding author. Tel: +86 411 84706337; fax: 86 411 84708400.
E-mail address: yzhao@dlut.edu.cn (Y. Zhao).

0022-460X/$ - see front matter © 2010 Elsevier Ltd. All rights reserved.
doi:10.1016/j.jsv.2010.05.004

structure of Wuhan light rail. Although the fixed-vehicle model can deal with the random vibration of vehicles, it does not perform satisfactorily when determining the responses of the track. These shortcomings can be overcome by using the more realistic moving-vehicle model which assumes motion along the track. However, this introduces time-dependent systems and as a result has rarely been used previously. Chen [1] and Lei and Noda [5] have used this model to analyze random responses of such coupled systems, including nonlinear contact springs to simulate the wheel–rail contact forces. Wang et al. [6] evaluated those parameters that influence train safety and comfort by analyzing a variety of trains running on a fixed track at different velocities for both passenger and freight traffic. Shi et al. [7] and Long et al. [8] applied this model to maglev and linear metro coupled vehicle–track systems, respectively, in order to analyze the dynamic responses excited by track irregularity. Such approaches necessitate the calculation of dynamic responses in the time domain, using a series of samples from the track irregularity PSD, before transformation into the frequency domain to obtain the response PSDs.

The purpose of the present paper is to extend the work of Lu et al. [3] by developing an efficient method for computing response PSDs of vehicle–track coupled systems using the moving-vehicle model. This introduces a time dependency into the problem, with the result that the responses of the coupled system are non-stationary, even if the excitations are stationary. This requires a very long section of track to be included in a conventional FE model to make the analysis reliable. For example, 500–600 degrees of freedom (dof) were used for the vertical response analysis in Refs. [1,5]. In addition, when solving the equation of motion by using a step-by-step integration method, a fairly long integral time is needed to reach steady state. In the case of high-speed trains, the high-frequency excitations quickly become more important, so structural models with higher dof and integration with shorter integral step, as well as longer integral time, need to be considered.

An overview of the way these difficulties are overcome in the present paper can be gleaned from the following four steps:

(1) Initially PEM [9–11] for fully coherent linear time-dependent structures is used to accelerate the calculation by transforming random excitations into harmonic pseudo-excitations.
(2) The track is then regarded as a periodic structure [12–14] and based on the theory of wave propagation in substructural chain-type structures [15–19], the symplectic mathematical scheme [20–24] is used to investigate the random wave propagation. This enables only those sections currently in contact with the vehicle to be included in the computation, which considerably reduces the computational effort, while retaining the accuracy due to symplectic characteristics.
(3) The equation of motion of the coupled system is then rewritten as a first order linear differential equation group with periodic coefficients in state-space and the expressions for its periodic state transition matrix and periodic load vector are then derived. According to the theory of differential equations [25], the solution of such a differential equation group is also periodic. By using this property and the Schur decomposition scheme, the step-by-step integration problem is transformed into a linear equation set with an upper triangular coefficient matrix.
(4) When using PEM, a series of pseudo-excitations at different frequencies need be dealt with. In order to avoid repeated computations, the frequency-dependent terms are separated from the load vector.

2. Pseudo-excitation method

The pseudo-excitation method is an accurate and highly efficient algorithm for structural stationary/non-stationary random response analysis. In the following section its algorithm for stationary fully coherent problems of linear time-dependent structures is outlined.

2.1. PEM for stationary fully coherent problems of linear time-dependent structures

If the auto-PSD and cross-PSD functions of excitations f_1 and f_2 satisfy the relationship

$$\frac{|S_{f_1f_2}(\omega)|^2}{S_{f_1f_1}(\omega)S_{f_2f_2}(\omega)}=\frac{|S_{f_2f_1}(\omega)|^2}{S_{f_1f_1}(\omega)S_{f_2f_2}(\omega)}=1 \tag{1}$$

then the two excitations are fully coherent [26]. Usually, multiple excitations caused by the same source, without noise interference, are fully coherent and in this case the random excitation vector $\mathbf{f}(t)$ can be expressed as

$$\mathbf{f}(t)=\left\{f(t-t_1)\quad f(t-t_2)\quad\cdots\quad f(t-t_m)\right\}^{\mathrm{T}} \tag{2}$$

Here $f(t)$ is the random excitation source. Without losing generality, let $t_1=0$, then t_j ($j=1,2,\ldots,m$) would be the time lag of the jth excitation with respect to the first one. The PSD of $f(t)$ is denoted as $S_f(\omega)$, where ω is circular frequency. The

input PSD matrix is then

$$\mathbf{S}_{\mathrm{in}}(\omega)=\begin{bmatrix} 1 & \mathrm{e}^{i\omega(t_1-t_2)} & \cdots & \mathrm{e}^{i\omega(t_1-t_m)} \\ \mathrm{e}^{i\omega(t_2-t_1)} & 1 & \cdots & \mathrm{e}^{i\omega(t_2-t_m)} \\ \vdots & \vdots & & \vdots \\ \mathrm{e}^{i\omega(t_m-t_1)} & \mathrm{e}^{i\omega(t_m-t_2)} & \cdots & 1 \end{bmatrix} S_f(\omega) \tag{3}$$

For a linear time-dependent structure subjected to the random excitation $\mathbf{f}(t)$, the corresponding response vector can be expressed by Duhamel's integral as

$$\mathbf{z}(t)=\int_0^t \mathbf{H}(t,\tau)\mathbf{f}(\tau)\,\mathrm{d}\tau \tag{4}$$

in which $\mathbf{H}(t,\tau)$ is the frequency response matrix. Multiplying $\mathbf{z}(t)$ by its transpose and applying the mathematical expectation operator, the variance matrix of the response vector can be obtained as

$$\mathbf{R}_{\mathbf{zz}}(t)=E[\mathbf{z}(t)\mathbf{z}^{\mathrm{T}}(t)]=\int_0^t\int_0^t \mathbf{H}(t,\tau_1)E[\mathbf{f}(\tau_1)\mathbf{f}^{\mathrm{T}}(\tau_2)]\mathbf{H}^{\mathrm{T}}(t,\tau_2)\,\mathrm{d}\tau_1\,\mathrm{d}\tau_2 \tag{5}$$

According to the Wiener–Khintchine theorem

$$E[\mathbf{f}(\tau_1)\mathbf{f}^{\mathrm{T}}(\tau_2)]=\int_{-\infty}^{+\infty}\mathbf{S}_{in}(\omega)\mathrm{e}^{i\omega(\tau_2-\tau_1)}\,\mathrm{d}\omega \tag{6}$$

Substituting Eq. (6) into Eq. (5) and exchanging the integral order gives the evolutionary PSD matrix of response vector $\mathbf{z}(t)$ as

$$\mathbf{R}_{\mathbf{zz}}(t)=\int_{-\infty}^{+\infty}\mathbf{S}_{\mathbf{zz}}(\omega,t)\,\mathrm{d}\omega \tag{7}$$

$$\mathbf{S}_{\mathbf{zz}}(\omega,t)=\int_0^t\int_0^t \mathbf{H}(t,\tau_1)\mathbf{S}_{\mathrm{in}}(\omega)\mathbf{H}^{\mathrm{T}}(t,\tau_2)\mathrm{e}^{i\omega(\tau_2-\tau_1)}\,\mathrm{d}\tau_1\,\mathrm{d}\tau_2 \tag{8}$$

It can be seen that Eq. (8) is a double integral expression which is very time consuming to compute directly. Therefore, PEM will be used instead. Assume that the structure is subjected to a pseudo-excitation

$$\tilde{\mathbf{f}}(\omega,t)=\left\{\mathrm{e}^{-i\omega t_1}\quad \mathrm{e}^{-i\omega t_2}\quad \cdots\quad \mathrm{e}^{-i\omega t_m}\right\}\sqrt{S_f(\omega)}\,\mathrm{e}^{i\omega t} \tag{9}$$

Eq. (8) can then be rewritten as

$$\mathbf{S}_{\mathbf{zz}}(\omega,t)=\tilde{\mathbf{z}}^{*}(\omega,t)\tilde{\mathbf{z}}^{\mathrm{T}}(\omega,t),\quad \tilde{\mathbf{z}}(\omega,t)=\int_0^t \mathbf{H}(t,\tau)\tilde{\mathbf{f}}(\omega,\tau)\,\mathrm{d}\tau \tag{10}$$

where the superscript * represents the complex conjugate. It is clear that $\tilde{\mathbf{z}}(\omega,t)$ is the response of the structure when it is subjected to the pseudo-excitation and that the first of Eqs. (10) has a much simpler form than Eq. (8). Thus, the use of PEM to transform random excitations into harmonic pseudo-excitations leads to a significant reduction in computational effort.

2.2. Application of PEM to coupled vehicle–track systems

The model for the random vibration analysis of the coupled vehicle–track system is shown in Fig. 1. The vehicle with four wheels is modelled as a spring–mass–damper system with 10 dof and the track is regarded as an infinitely long substructural chain consisting of three layers, i.e. the rails, sleepers and ballast. The vehicle and the track are coupled via linear springs [1] of stiffness $k_h=1.5P_0^{1/3}/G$, where P_0 is the static wheel–rail force and G is a contact constant. Assume that the vehicle is moving at velocity v on the track whose irregularity, $r(x)$, varies with distance $x(t)$ and can be regarded as a zero-mean valued stationary random process with PSD $S_{rr}^{s}(\Omega)$ known, where Ω is the spatial frequency. In the time domain, this corresponds to a PSD of track irregularity $r(t)$ of $S_{rr}^{t}(\omega)=S_{rr}^{s}(\Omega)/v$. The random excitations applied to the wheels by the track can be expressed by the vector

$$\mathbf{f}=\mathbf{\Gamma}(t)\mathbf{r}(t) \tag{11}$$

in which $\mathbf{\Gamma}(t)$ varies with the vehicle position and $\mathbf{r}(t)$ is a vector of track irregularities at the wheel–rail contact points, given by

$$\mathbf{r}(t)=\left\{r(t-t_1)\quad r(t-t_2)\quad r(t-t_3)\quad r(t-t_4)\right\}^{\mathrm{T}} \tag{12}$$

where

$$t_1=0,\quad t_2=2l_t/v,\quad t_3=2l_c/v,\quad t_4=2(l_t+l_c)/v \tag{13}$$

Here $2l_t$ and $2l_c$ are the wheel pair and bogie spacing, respectively. According to PEM, the pseudo-excitation can be defined as

$$\tilde{\mathbf{f}}(t)=\mathbf{\Gamma}(t)\left\{\begin{array}{cccc} e^{-i\omega t_1} & e^{-i\omega t_2} & e^{-i\omega t_3} & e^{-i\omega t_4}\end{array}\right\}^{\mathrm{T}}\sqrt{S_{rr}(\omega)}e^{i\omega t} \tag{14}$$

This excitation can then be used with the equation of motion to determine the pseudo-response of the system. The corresponding PSDs and standard deviation follow directly using PEM.

3. Symplectic analysis for infinitely long substructural chain

In this section, the symplectic mathematical scheme is generalized for the first time to investigate the random wave propagation, as follows. Consider the infinitely long substructural chain of Fig. 2, which consists of unloaded identical substructures, denoted as sub; and the loaded, but otherwise identical substructure sub*, which is subjected to an arbitrary load $\mathbf{f}(t)$. The equation of motion of the loaded substructure is

$$\mathbf{M}\ddot{\mathbf{y}}+\mathbf{C}\dot{\mathbf{y}}+\mathbf{K}\mathbf{y}=\mathbf{f}(t)+\mathbf{f}_b \tag{15}$$

in which

$$\mathbf{y}=\left\{\begin{array}{ccc}\mathbf{y}_a^{\mathrm{T}} & \mathbf{y}_b^{\mathrm{T}} & \mathbf{y}_i^{\mathrm{T}}\end{array}\right\}^{\mathrm{T}},\quad \mathbf{f}_b=\left\{\begin{array}{ccc}\mathbf{p}_a^{\mathrm{T}} & -\mathbf{p}_b^{\mathrm{T}} & \mathbf{p}_i^{\mathrm{T}}\end{array}\right\}^{\mathrm{T}} \tag{16}$$

where $\mathbf{y}_a$ and $\mathbf{y}_b$ are the displacement vectors at the left- and right-hand interfaces and $\mathbf{y}_i$ is the internal displacement vector and; $\mathbf{P}_a$, $\mathbf{P}_b$ and $\mathbf{P}_i$ are the corresponding nodal force vectors. For a typical undamped substructure without external

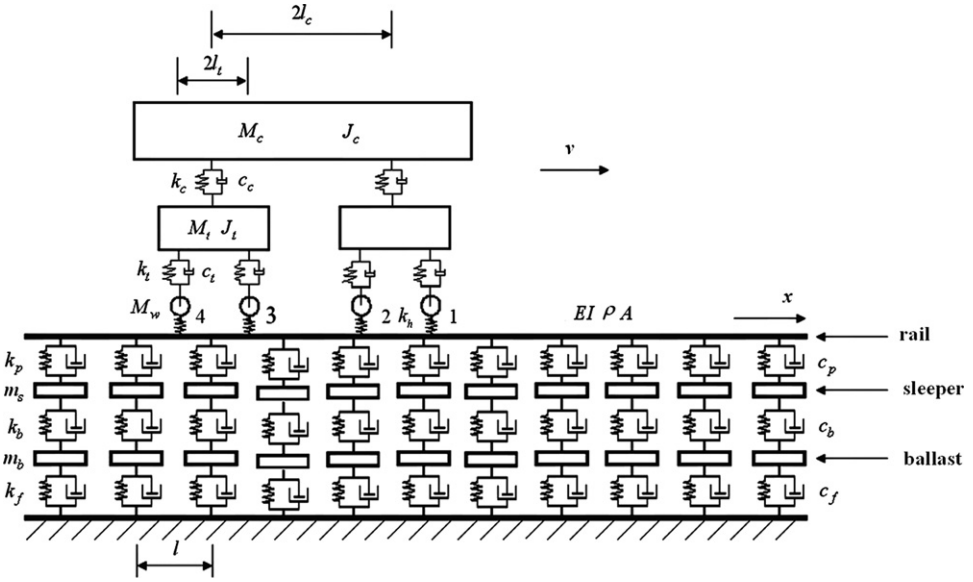

Fig. 1. Model of coupled vehicle–track system.

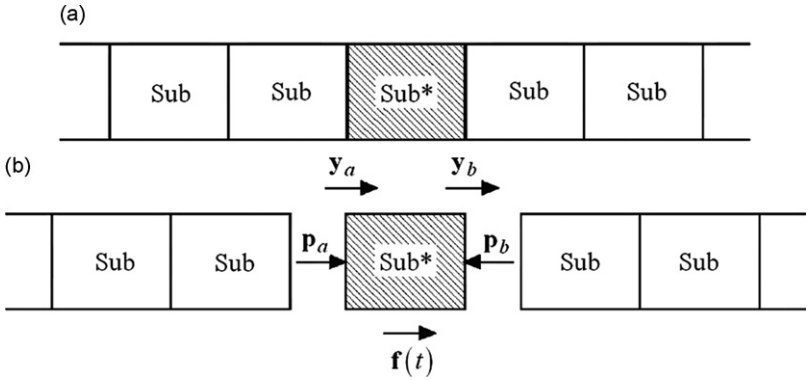

Fig. 2. Infinitely long substructural chain.

excitation, it has been proven [22] that

$$\begin{Bmatrix} \mathbf{y}_b \\ \mathbf{p}_b \end{Bmatrix} = \mathbf{D} \begin{Bmatrix} \mathbf{y}_a \\ \mathbf{p}_a \end{Bmatrix} = \mu \begin{Bmatrix} \mathbf{y}_a \\ \mathbf{p}_a \end{Bmatrix} \tag{17}$$

in which $\mathbf{D}(\omega)$ is a symplectic transfer matrix that satisfies the equation

$$\mathbf{D}^{\mathrm{T}}\mathbf{J}_n\mathbf{D} = \mathbf{J}_n, \quad \mathbf{J}_n = \begin{bmatrix} \mathbf{0} & \mathbf{I}_n \\ -\mathbf{I}_n & \mathbf{0} \end{bmatrix}, \quad \mathbf{J}_n^{\mathrm{T}} = \mathbf{J}_n^{-1} = -\mathbf{J}_n \tag{18}$$

where $\mathbf{I}_n$ is the n-dimensional unit matrix; and if μ is an eigenvalue of $\mathbf{D}(\omega)$, then so is $1/\mu$. These eigenvalues are called wave propagation constants and $|\mu|=1$ refers to transmission waves that propagate without decay at frequencies that lie within the frequency passband [9]. For such a periodic structure, there are infinitely many transmission frequencies. Since $|\mu|=1$, we can assume $\mu=e^{i\theta}$ and select a finite number of θ_j ($j=1,2,\ldots,m$) evenly in the interval $[0, 2\pi)$ to calculate the responses. For each corresponding wave propagation constant μ_j ($j=1,2,\ldots,m$), it can be verified that

$$\begin{Bmatrix} \mathbf{y}_a \\ \mathbf{y}_b \\ \mathbf{y}_i \end{Bmatrix} = \begin{bmatrix} \mathbf{I} & \mathbf{0} \\ \mu_j\mathbf{I} & \mathbf{0} \\ \mathbf{0} & \mathbf{I} \end{bmatrix} \begin{Bmatrix} \mathbf{y}_a \\ \mathbf{y}_i \end{Bmatrix} = \mathbf{T}_j \begin{Bmatrix} \mathbf{y}_a \\ \mathbf{y}_i \end{Bmatrix}$$
$$\mathbf{T}_j^{\mathrm{H}}\mathbf{f}_b = \begin{bmatrix} \mathbf{I} & \mu_j^{-1}\mathbf{I} & \mathbf{0} \\ \mathbf{0} & \mathbf{0} & \mathbf{I} \end{bmatrix} \begin{Bmatrix} \mathbf{p}_a \\ -\mathbf{p}_b \\ \mathbf{0} \end{Bmatrix} = \begin{Bmatrix} \mathbf{p}_a - \mu_j^{-1}\mathbf{p}_b \\ \mathbf{0} \end{Bmatrix} = \begin{Bmatrix} \mathbf{0} \\ \mathbf{0} \end{Bmatrix} \tag{19}$$

By using the complete set of eigenvectors $\mathbf{\Psi}_j$ associated with the μ_j, the mode-superposition equation can be written as

$$\mathbf{y}_j = \mathbf{T}_j\mathbf{\Psi}_j\mathbf{q}_j \tag{20}$$

The response of the kth substructure is then given by

$$\mathbf{y}_k = \frac{1}{m}\sum_{j=1}^{m}\mu_j^k\mathbf{y}_j = \frac{1}{m}\sum_{j=1}^{m}\mu_j^k\mathbf{T}_j\mathbf{\Psi}_j\mathbf{q}_j \tag{21}$$

where $k=0$ corresponds to the loaded substructure, $k>0$ to the substructures to its right and $k<0$ to the substructures to its left. The $\mathbf{\Psi}_j$ can be obtained by solving the following generalized eigenproblem

$$\mathbf{T}_j^{\mathrm{H}}\mathbf{K}\mathbf{T}_j\mathbf{\Psi}_j = \mathbf{T}_j^{\mathrm{H}}\mathbf{M}\mathbf{T}_j\mathbf{\Psi}_j\mathbf{\Omega}_j^2 \tag{22}$$

Substituting Eqs. (20) and (21) into Eq. (15) and multiplying both sides by $\mathbf{\Psi}_j^{\mathrm{H}}\mathbf{T}_j^{\mathrm{H}}$ gives

$$\mathbf{M}_j\ddot{\mathbf{q}}_j + \mathbf{C}_j\dot{\mathbf{q}}_j + \mathbf{K}_j\mathbf{q}_j = \mathbf{\Psi}_j^{\mathrm{H}}\mathbf{T}_j^{\mathrm{H}}\mathbf{f}(t) \tag{23}$$

in which

$$\mathbf{M}_j = \mathbf{\Psi}_j^{\mathrm{H}}\mathbf{T}_j^{\mathrm{H}}\mathbf{M}\mathbf{T}_j\mathbf{\Psi}_j, \quad \mathbf{C}_j = \mathbf{\Psi}_j^{\mathrm{H}}\mathbf{T}_j^{\mathrm{H}}\mathbf{C}\mathbf{T}_j\mathbf{\Psi}_j, \quad \mathbf{K}_j = \mathbf{\Psi}_j^{\mathrm{H}}\mathbf{T}_j^{\mathrm{H}}\mathbf{K}\mathbf{T}_j\mathbf{\Psi}_j \tag{24}$$

Combining the equations corresponding to each of the m propagation constants gives

$$\overline{\mathbf{M}}\ddot{\mathbf{q}} + \overline{\mathbf{C}}\dot{\mathbf{q}} + \overline{\mathbf{K}}\mathbf{q} = \overline{\mathbf{f}} \tag{25}$$

4. Equation of motion of the coupled vehicle–track system

In this section, the equation of motion for the coupled vehicle–track system excited by the harmonic pseudo-excitations is established.

4.1. Equation of motion of the vehicle

The equation of motion of the vehicle is

$$\mathbf{M}_v\ddot{\mathbf{y}}_v + \mathbf{C}_v\dot{\mathbf{y}}_v + \mathbf{K}_v\mathbf{y}_v = \mathbf{f}_v \tag{26}$$

where

$$\mathbf{f}_v = \begin{Bmatrix} 0 & 0 & 0 & 0 & 0 & 0 & f_{w1} & f_{w2} & f_{w3} & f_{w4} \end{Bmatrix}^{\mathrm{T}} \tag{27}$$

Here $\mathbf{M}_v$, $\mathbf{C}_v$ and $\mathbf{K}_v$ are the mass, damping and stiffness matrices of the vehicle; $\mathbf{y}_v$ is the vertical displacement vector and; f_{wi} ($i=1,2,3,4$) are the wheel–rail forces.

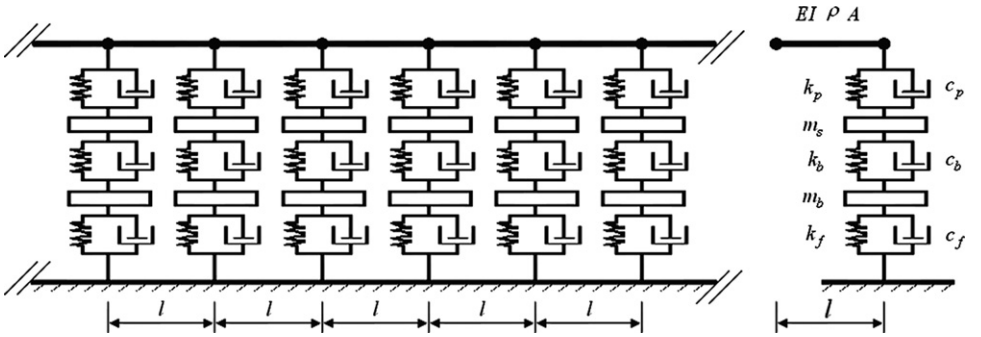

Fig. 3. A substructure of the track.

4.2. Equation of motion of the track

Each substructure of the track consists of a pair of rail sections, idealised as a single Bernoulli–Euler beam element between two adjacent sleepers, one of the two sleepers and the corresponding ballast segment are shown in Fig. 3. For the loaded substructure in contact with the ith wheel pair, the equation of motion is

$$\mathbf{M}_t\ddot{\mathbf{y}}_i+\mathbf{C}_t\dot{\mathbf{y}}_i+\mathbf{K}_t\mathbf{y}_i=\mathbf{N}(\xi_i)f_{wi}+\mathbf{f}_{bi} \tag{28}$$

where $\mathbf{y}_i$ is the displacement vector of the substructure; $\mathbf{f}_{bi}$ is its boundary force vector and $\mathbf{N}(\xi_i)$ is the shape function vector of the Bernoulli–Euler beam element, where the ξ_i are the dimensionless natural coordinates of the wheel–rail contact points that vary with distance $x(t)$. Proceeding in the same ways as Section 3, it is possible to write Eq. (28) in the form of Eq. (25) as

$$\overline{\mathbf{M}}_t\ddot{\mathbf{q}}_i+\overline{\mathbf{C}}_t\dot{\mathbf{q}}_i+\overline{\mathbf{K}}_t\mathbf{q}_i=\overline{\mathbf{f}}_i \quad (i=1,2,3,4) \tag{29}$$

It should be noted that, when solving Eq. (29) using step-by-step integration, the integral initial value can be determined from Eq. (21) if one of the wheels moves to the adjacent substructure.

4.3. Equation of motion of coupled vehicle–track systems

When the coupled system is subjected to the pseudo-excitation presented in Section 2.2, the wheel–rail force can be expressed as

$$\tilde{f}_{wi}=k_h\left(\tilde{y}_{ri}^w-\tilde{y}_{vi}^w+\sqrt{S_{rr}}\,\mathrm{e}^{\mathrm{i}\omega(t-t_i)}\right) \tag{30}$$

where $\tilde{y}_{vi}^w$and $\tilde{y}_{ri}^w$ are the pseudo-displacements of the wheels and rails at the wheel–rail contact point. As the track is subject to four wheel–rail forces, any displacement of the ith substructure can be obtained as the sum of the responses $\tilde{\mathbf{y}}_{ki}$ caused by each of the wheel–rail forces, i.e.

$$\tilde{\mathbf{y}}_i^t=\sum_{k=1}^{4}\tilde{\mathbf{y}}_{ki} \tag{31}$$

According to Ref. [1], the effective range of the wheel–rail force on the track is about 10 sleeper spacings, so any influences exceeding this range are ignored. In this way $\tilde{y}_{ri}^w$ can be obtained from the following equation:

$$\tilde{y}_{ri}^w=\mathbf{N}^{\mathrm{T}}(\xi_i)\tilde{\mathbf{y}}_i^t \tag{32}$$

Substituting Eqs. (30)–(32) into Eqs. (26)–(29) and combining them into a single equation gives the equation of motion of the coupled system as

$$\begin{bmatrix}\mathbf{M}_v & \\ & \mathbf{M}_t^*\end{bmatrix}\begin{Bmatrix}\ddot{\tilde{\mathbf{y}}}_v\\ \ddot{\tilde{\mathbf{q}}}\end{Bmatrix}+\begin{bmatrix}\mathbf{C}_v & \\ & \mathbf{C}_t^*\end{bmatrix}\begin{Bmatrix}\dot{\tilde{\mathbf{y}}}_v\\ \dot{\tilde{\mathbf{q}}}\end{Bmatrix}+\begin{bmatrix}\mathbf{K}_v & -\mathbf{R}_v\\ -\mathbf{R}_0 & \mathbf{K}_t^*-\mathbf{R}_t\end{bmatrix}\begin{Bmatrix}\tilde{\mathbf{y}}_v\\ \tilde{\mathbf{q}}\end{Bmatrix}=\begin{Bmatrix}\mathbf{F}_v\\ \mathbf{F}_t\end{Bmatrix}\mathbf{E}\sqrt{S}\mathrm{e}^{\mathrm{i}\omega t} \tag{33}$$

where $\tilde{\mathbf{q}}=\{\tilde{\mathbf{q}}_1^{\mathrm{T}}\ \tilde{\mathbf{q}}_2^{\mathrm{T}}\ \tilde{\mathbf{q}}_3^{\mathrm{T}}\ \tilde{\mathbf{q}}_4^{\mathrm{T}}\}^{\mathrm{T}}$ is the pseudo-generalized displacement vector of the track

$$\mathbf{M}_t^*=\begin{bmatrix}\overline{\mathbf{M}}_t & & & \\ & \overline{\mathbf{M}}_t & & \\ & & \overline{\mathbf{M}}_t & \\ & & & \overline{\mathbf{M}}_t\end{bmatrix},\quad \mathbf{C}_t^*=\begin{bmatrix}\overline{\mathbf{C}}_t & & & \\ & \overline{\mathbf{C}}_t & & \\ & & \overline{\mathbf{C}}_t & \\ & & & \overline{\mathbf{C}}_t\end{bmatrix},\quad \mathbf{K}_t^*=\begin{bmatrix}\overline{\mathbf{K}}_t & & & \\ & \overline{\mathbf{K}}_t & & \\ & & \overline{\mathbf{K}}_t & \\ & & & \overline{\mathbf{K}}_t\end{bmatrix},\quad \mathbf{E}=\begin{Bmatrix}\mathrm{e}^{-\mathrm{i}\omega t_1}\\ \mathrm{e}^{-\mathrm{i}\omega t_2}\\ \mathrm{e}^{-\mathrm{i}\omega t_3}\\ \mathrm{e}^{-\mathrm{i}\omega t_4}\end{Bmatrix} \tag{34}$$

where $\mathbf{R}_v$, $\mathbf{R}_0$ and $\mathbf{R}_t$ are time-dependent matrices and $\mathbf{F}_v$ and $\mathbf{F}_t$ are load coefficient matrices. Since these equations all share the same shape function $\mathbf{N}(\xi_i)$ and are periodic, Eq. (33) can be written in the form

$$\mathbf{M}_s\ddot{\tilde{\mathbf{y}}}_s+\mathbf{C}_s\dot{\tilde{\mathbf{y}}}_s+\mathbf{K}_s(t)\tilde{\mathbf{y}}_s=\mathbf{F}_s(t)\mathbf{E}(\omega,\nu)\sqrt{S}\mathrm{e}^{\mathrm{i}\omega t} \tag{35}$$

where

$$\mathbf{K}_s(t+T)=\mathbf{K}_s(t),\quad \mathbf{F}_s(t+T)=\mathbf{F}_s(t) \tag{36}$$

and the period $T=l/v$, where l is the sleeper spacing.

5. Solution of the coupled vehicle–track system

5.1. Periodic state transition matrix and periodic load vector

Eq. (35) can be transformed to state-space as

$$\dot{\tilde{\mathbf{v}}}=\mathbf{H}(t)\tilde{\mathbf{v}}+\tilde{\mathbf{f}}(\omega,t) \tag{37}$$

where

$$\tilde{\mathbf{v}}=\begin{Bmatrix}\tilde{\mathbf{y}}_s\\ \dot{\tilde{\mathbf{y}}}_s\end{Bmatrix},\quad \mathbf{H}(t)=\begin{bmatrix}\mathbf{0} & \mathbf{I}\\ -\mathbf{M}_s^{-1}\mathbf{K}_s(t) & -\mathbf{M}_s^{-1}\mathbf{C}_s\end{bmatrix},\quad \tilde{\mathbf{f}}(\omega,t)=\begin{bmatrix}\mathbf{0}\\ \mathbf{M}_s^{-1}\mathbf{F}_s(t)\end{bmatrix}\mathbf{E}(\omega,\nu)\sqrt{S}\mathrm{e}^{\mathrm{i}\omega t} \tag{38}$$

Usually, Eq. (37) is solved using a step-by-step integration scheme. Thus if the response at time t_k is denoted by $\tilde{\mathbf{v}}_k$, the response at time t_{k+1} can be expressed as

$$\tilde{\mathbf{v}}_{k+1}=\mathbf{\Phi}[t_{k+1},t_k]\tilde{\mathbf{v}}_k+\tilde{\mathbf{r}}_k,\quad \tilde{\mathbf{r}}_k=\mathbf{R}_k\mathbf{E}(\omega,\nu)\sqrt{S}\mathrm{e}^{\mathrm{i}\omega t_k} \tag{39}$$

where $\mathbf{\Phi}[*]$ denotes the state transition matrix, which has the property

$$\mathbf{\Phi}[t_a,t_b]=\mathbf{\Phi}[t_a,t_c]\mathbf{\Phi}[t_c,t_b] \tag{40}$$

Assume now that s integration steps are adopted in one period. If the initial value is denoted by $\tilde{\mathbf{v}}(t_0)=\tilde{\mathbf{v}}_0$ and the terminal value by $\tilde{\mathbf{v}}(t_0+T)=\tilde{\mathbf{v}}_T$, Eqs. (39) and (40) yield

$$\tilde{\mathbf{v}}_T=\mathbf{\Phi}[t_0+T,t_0]\tilde{\mathbf{v}}_0+\tilde{\mathbf{r}}_T \tag{41}$$

in which

$$\mathbf{\Phi}[t_0+T,t_0]=\prod_{i=s-1}^{0}\mathbf{\Phi}[t_{i+1},t_i],\quad \tilde{\mathbf{r}}_T=\sum_{k=0}^{s-2}\left(\prod_{i=s-1}^{k+1}\mathbf{\Phi}[t_{i+1},t_i]\right)\tilde{\mathbf{r}}_k+\tilde{\mathbf{r}}_{s-1} \tag{42}$$

are the periodic state transition matrix and the periodic load vector, respectively.

5.2. Solution for the periodic state transition matrix and periodic load vector

It can be seen from the first of each of Eqs. (39) and (42) that the periodic state transition matrix $\mathbf{\Phi}[t_0+T, t_0]$ is constant and therefore only needs to be calculated once. However, its calculation requires multiple matrix multiplications. If the size of the FE model is very large, as is the case when high-frequency components must be included, this calculation would be quite costly. It is therefore desirable to adopt a new method to calculate $\mathbf{\Phi}[t_0+T, t_0]$, as follows. Let

$$\tilde{\mathbf{v}}_0=\mathbf{I},\quad \tilde{\mathbf{r}}_T=\mathbf{0} \tag{43}$$

where $\boldsymbol{I}$ is a unit matrix with the same order as $\mathbf{\Phi}[t_0+T, t_0]$. Substituting Eq. (43) into Eq. (41) then gives

$$\tilde{\mathbf{v}}_T=\mathbf{\Phi}[t_0+T,t_0] \tag{44}$$

Consequently, $\mathbf{\Phi}[t_0+T, t_0]$ can be computed using the following algorithm: (1) take each column of the unit matrix $\mathbf{I}$ in turn and assume it to be the initial value of the coupled system response; (2) solve Eq. (35) using Newmark's method to obtain the response after one period, assuming the load vectors to be zero at all times; (3) update the corresponding columns of $\mathbf{\Phi}[t_0+T, t_0]$. Note that care must be taken to allow for the possibility of a wheel pair moving on to an adjacent substructure.

On the other hand, it can be seen from the second of each of Eqs. (39) and (42) that the periodic load vector $\tilde{\mathbf{r}}_T$ is related to load frequency. Thus when using PEM, which requires a series of pseudo-excitations at different frequencies to be imposed, it is important to avoid repeated computations. This can be achieved as follows. In the second of Eqs. (39) denote the factors related to load frequency by $\mathbf{g}_k$, i.e.

$$\mathbf{E}(\omega,\nu)\sqrt{S}\mathrm{e}^{\mathrm{i}\omega t_k}=\mathbf{g}_k\quad (k=0,1,\ldots,s-1) \tag{45}$$

Then substituting the second of Eqs. (39) into the second of Eqs. (42) gives

$$\tilde{\mathbf{r}}_T = \sum_{k=0}^{s-2}\left(\prod_{i=s-1}^{k+1}\mathbf{\Phi}[t_{i+1},t_i]\right)\mathbf{R}_k\mathbf{g}_k + \mathbf{R}_{s-1}\mathbf{g}_{s-1} = \sum_{k=0}^{s-1}\mathbf{G}_k\mathbf{g}_k \tag{46}$$

In Eq. (46) the factors related to load frequency have been separated from the others, so $\mathbf{G}_k(k=0,1,\ldots,s-1)$ need be calculated only once in order to obtain the periodic load vector $\tilde{\mathbf{r}}_T$. This can be achieved in a similar way to the solution of $\mathbf{\Phi}[t_0+T, t_0]$. Let

$$\tilde{\mathbf{v}}_0 = \mathbf{0}, \quad \mathbf{g}_k = \begin{cases} 1 & k=j \\ 0 & k\neq j \end{cases} \quad (j=0,1,\ldots,s-1) \tag{47}$$

Substituting Eq. (47) into Eqs. (41) and (46) gives

$$\tilde{\mathbf{v}}_T = \mathbf{G}_j \tag{48}$$

$\tilde{\mathbf{r}}_T$ can then be computed by using the following algorithm: (1) assume the initial value of the coupled system response vector is zero; (2) for each $j(j=0,1,\ldots,s-1)$, take each column of $\mathbf{F}_s(t_j)$ as the load vector at time t_j, while assuming the load vectors at other times be zero, and then solve Eq. (35) by using Newmark's method to obtain the response after one period; (3) update the corresponding columns of $\mathbf{G}_j$ and; (4) calculate the periodic load vector $\tilde{\mathbf{r}}_T$ subject to different pseudo-excitations according to Eq. (46).

During the above calculation, the scheme for vehicle–bridge interaction analysis was performed according to Yang and Wu [27].

5.3. Periodicity of the response of the coupled system

Assume that the pseudo-response of the coupled system can be expressed in the following form:

$$\tilde{\mathbf{v}} = \bar{\mathbf{v}}e^{i\omega t}, \quad \dot{\tilde{\mathbf{v}}} = (\dot{\bar{\mathbf{v}}} + i\omega\bar{\mathbf{v}})e^{i\omega t} \tag{49}$$

Substituting Eq. (49) into Eq. (37) gives

$$\dot{\bar{\mathbf{v}}} = (\mathbf{H}(t) - i\omega\mathbf{I})\bar{\mathbf{v}} + \mathbf{F}(t)\mathbf{E}(\omega,\nu)\sqrt{S} = \mathbf{A}(t)\bar{\mathbf{v}} + \mathbf{a}(t) \tag{50}$$

According to Eqs. (36) and (38), $\mathbf{A}(t)$ and $\mathbf{a}(t)$ are periodic

$$\mathbf{A}(t+T) = \mathbf{A}(t), \quad \mathbf{a}(t+T) = \mathbf{a}(t) \tag{51}$$

Thus, Eq. (50) is a differential equation group with periodic coefficients and therefore has a periodic solution [25], i.e.

$$\bar{\mathbf{v}}(t+T) = \bar{\mathbf{v}}(t) \tag{52}$$

Clearly, Eqs. (51) and (52) are not valid if PEM is not used.

5.4. Response of the coupled vehicle–track system

Without losing generality, let t_0=0 and substitute Eqs. (49) and (52) into Eq. (41) to give

$$(\mathbf{I}e^{i\omega T} - \mathbf{\Phi}[T,0])\bar{\mathbf{v}}(0) = \tilde{\mathbf{r}}_T \tag{53}$$

where $\mathbf{\Phi}[T, 0]$ is the periodic state transition matrix, which is usually a full matrix. Hence the coefficient matrix of Eq. (53) is also a full matrix and is related to the load frequency. A large amount of computational effort is then required if Eq. (53) is solved directly at different frequencies. Improved efficiency in this area can be achieved by performing a Schur decomposition scheme on $\mathbf{\Phi}[T, 0]$, i.e.

$$\mathbf{\Phi}[T,0] = \mathbf{U}\mathbf{T}\mathbf{U}^{\mathrm{T}}, \quad \mathbf{U}\mathbf{U}^{\mathrm{T}} = \mathbf{I} \tag{54}$$

where $\mathbf{U}$ is an orthogonal matrix and $\mathbf{T}$ is an upper triangular matrix. Substituting Eq. (54) into Eq. (53) gives

$$(\mathbf{I}e^{i\omega T} - \mathbf{T})\mathbf{U}^{\mathrm{T}}\bar{\mathbf{v}}(0) = \mathbf{U}^{\mathrm{T}}\tilde{\mathbf{r}}_T \tag{55}$$

The following change of variable

$$\bar{\mathbf{w}} = \mathbf{U}^{\mathrm{T}}\bar{\mathbf{v}} \tag{56}$$

allows Eq. (55) to be written as

$$(\mathbf{I}e^{i\omega T} - \mathbf{T})\bar{\mathbf{w}}(0) = \mathbf{U}^{\mathrm{T}}\tilde{\mathbf{r}}_T \tag{57}$$

Thus, the original step-by-step integration problem is transformed into a linear equation set with an upper triangular coefficient matrix that yields $\bar{\mathbf{w}}(0)$ from Eq. (57). Considering the orthogonality of matrix $\mathbf{U}$, Eqs. (49) and (56) lead to

$$\tilde{\mathbf{v}}(0) = \bar{\mathbf{v}}(0) = \mathbf{U}\bar{\mathbf{w}}(0) \tag{58}$$

Since the pseudo-responses $\tilde{\mathbf{v}}(0)$ at time $t=0$ have already been obtained, it is not difficult to calculate the pseudo-responses at other times. Denoting the pseudo-response of the variable $u(t)$ as $\tilde{u}(\omega,t)$ and utilising PEM, the PSD of $u(t)$ can be written as

$$S(\omega,t)=\tilde{u}(\omega,t)\tilde{u}^{*}(\omega,t) \tag{59}$$

6. Numerical examples

The parameters of the high-speed train manufactured in the Changchun Railroad Carriage Manufacturing Plant are listed in Table 1 [1] and the track parameters are listed in Table 2. As only a half vehicle–track model is employed, some of the parameters must be halved in the calculation. The American track spectrum, i.e. function (a) of Eq. (60), will be adopted when the track wavelength is longer than 1 m; otherwise function (b) of Eq. (60) proposed by the Chinese Railway Science Academy [1] will be used. In these two functions k, A_v and Ω_c take different values for different classes of track, as listed in Table 3

$$\begin{aligned}&(a)\quad S_r(\Omega)=\frac{kA_v\Omega_c^2}{\Omega^2(\Omega^2+\Omega_c^2)}\,(\mathrm{cm}^2/\mathrm{rad}/m)\\&(b)\quad S_r(f)=0.036f^{-3.15}\,(\mathrm{mm}^2/\mathrm{cycle}/m)\end{aligned} \tag{60}$$

The responses of the sleepers beneath the first wheel pair are now investigated. American track spectrum class 6 and vehicle velocity of 100 km/h are assumed in the calculation unless specified otherwise.

6.1. Comparison with a Monte-Carlo simulation

This simulation firstly generates a large number of track irregularity samples in the time domain using the track profile irregularity PSD. The responses of the coupled vehicle–track system are then calculated for each sample, before final transformation into the frequency domain to obtain the response PSDs. Table 4 lists the standard deviations of the coupled system as well as the computation times. Since a Monte-Carlo simulation is performed in the time domain, its results will fluctuate with time. Hence the results listed are the mean values and the fluctuation ranges of the responses with the first wheel pair passing through 50 sleepers during a steady running state. It can be seen that if the sample number is 5, the mean values differ substantially from the results given by the proposed method. If the number of samples is increased

Table 1
Vehicle parameters.

Vehicle body mass, M_c	34×10^3 kg	Primary suspension, c_t	6×10^3 N s/m
Vehicle body inertia, J_c	2.277×10^6 kg m^2	Secondary suspension, k_c	400×10^3 N/m
Bogie mass, M_t	3000 kg	Secondary suspension, c_c	80×10^3 N s/m
Bogie inertia, J_t	2710 kg m^2	Wheelset spacing, $2l_t$	2.4 m
Wheelset mass, M_w	1400 kg	Bogie spacing, $2l_c$	18 m
Primary suspension, k_t	550×10^3 N/m	Contact constant, G	5.135×10^3 m/N$^{2/3}$

Table 2
Track parameters.

Rail bending stiffness, EI	6.62×10^6 N m^2	Ballast stiffness, k_b	1.82×10^8 N/m
Linear density of rail, ρA	60.64 kg/m	Subgrade stiffness, k_f	1.47×10^8 N/m
Sleeper spacing, l	0.545 m	Railpad damping, c_p	7.5×10^4 N s/m
Sleeper mass, m_s	237 kg	Ballast damping, c_b	5.88×10^4 N s/m
Ballast mass, m_b	1478 kg	Subgrade damping, c_f	3.115×10^4 N s/m
Railpad stiffness, k_p	1.2×10^8 N/m		

Table 3
Parameters for the American track spectrum.

Parameter	Value		
	Class 6	Class 5	Class 4
k	0.25	0.25	0.25
A_v	0.0339	0.2095	0.5376
Ω_c	0.8245	0.8245	0.8245

Table 4
Comparison between the proposed method and Monte-Carlo simulation with the number of samples shown in italics.

	The proposed method		Monte-Carlo simulation			
	Standard deviation	CPU time (s)	Standard deviation			CPU time (s) (*100*)
			5	*20*	*100*	
Body acceleration	0.1126	0.968	0.0861 ± 0.0352	0.1086 ± 0.0524	0.1092 ± 0.0139	6085
1st bogie acceleration	0.4388	1.953	0.3703 ± 0.4088	0.3979 ± 0.2097	0.4387 ± 0.0826	6194
Sleeper acceleration	38.7380	3.922	34.7361 ± 36.3041	37.7349 ± 19.4098	38.7229 ± 5.6498	7319
Ballast acceleration	20.315	3.922	16.1386 ± 13.0708	19.3537 ± 10.0375	20.3633 ± 2.7547	6083
1st wheel–rail force	26,189	21.20	$18{,}003 \pm 21{,}720$	$25{,}506 \pm 8005$	$26{,}502 \pm 3427$	15,596

The units of the standard deviations are N for the last row and m/s^2 else where.

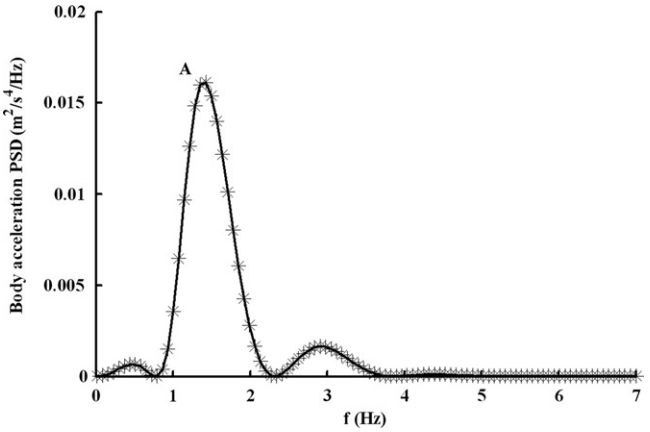

Fig. 4. PSD of vehicle body vertical acceleration.

to 20, the mean values given by the two methods agree only slightly better, and the fluctuation ranges are still too large. A further increase to 100 samples yields results that agree to at least a tolerable level, which justifies the correctness of the proposed method, although the fluctuations are still around 10–20%. Clearly, many more samples would be required to obtain satisfactory results from the Monte-Carlo method; however, the effort required would be unacceptable.

The CPU times for the proposed method and the Monte-Carlo simulation with 100 samples are also listed in Table 4. In the calculation, the parameter m takes the value of 10 when calculating the responses of the vehicle body and bogies, and 20 for other responses. For the responses calculated, the closer their locations are to the wheel–rail contact points, the more frequencies associated with the pseudo-excitations are required to ensure suitable accuracy. In similar fashion, shorter integral steps and longer integral time are required for the Monte-Carlo simulation. As discussed in Section 5.2, the periodic state transition matrix $\mathbf{\Phi}[t_0+T,t_0]$ and the matrices $\mathbf{G}_k(k=0,1,\ldots,s-1)$ in Eq. (46) only need to be calculated once for each value of m, which takes 69.9 s or 423.6 s for $m=10$ or 20, and this result can be used directly when calculating the responses of the coupled system.

6.2. Comparison between the two excitation models

In this example, the fixed-vehicle model and the moving-vehicle model are compared. The responses of the fixed-vehicle model are given by the solid line, while those of the moving-vehicle model are given by the asterisks in Figs. 4 and 5 and by the dotted line in Fig. 6.

Fig. 4 gives the PSD curves of the vehicle body vertical acceleration, which show that the results calculated by the two models agree very well. The peak values at point A are $1.614036 \times 10^{-2}\ m^2/s^4/Hz$ for the fixed-vehicle model and $1.614070 \times 10^{-2}\ m^2/s^4/Hz$ for the moving-vehicle model, an error of only 0.0021%. The bogie acceleration PSD curves calculated by the two models are equally close, but are not given in the figures. Fig. 5 gives the PSD curves of the 1st and 2nd wheel–rail contact forces. It can be seen from Fig. 5(a) that the PSD curves of the 1st wheel–rail contact force are still reasonably close to each other. The peak values at point B are $4.055 \times 10^7\ N^2/Hz$ for the fixed-vehicle model and $4.1143 \times 10^7\ N^2/Hz$ for the moving-vehicle model, an error of 1.44%. However, a much bigger difference exists between the PSD curves of the 2nd wheel–rail contact force, as shown in Fig. 5(b). The peak values at point C are $3.1681 \times 10^7\ N^2/Hz$ for

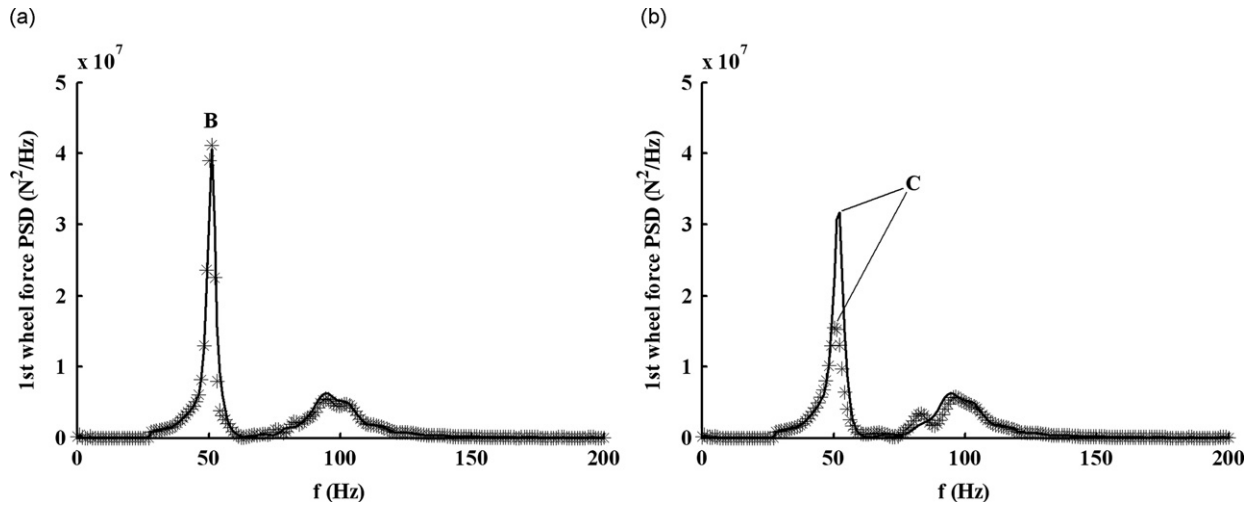

Fig. 5. PSDs of rail–wheel contact force: (a) 1st wheel and (b) 2nd wheel.

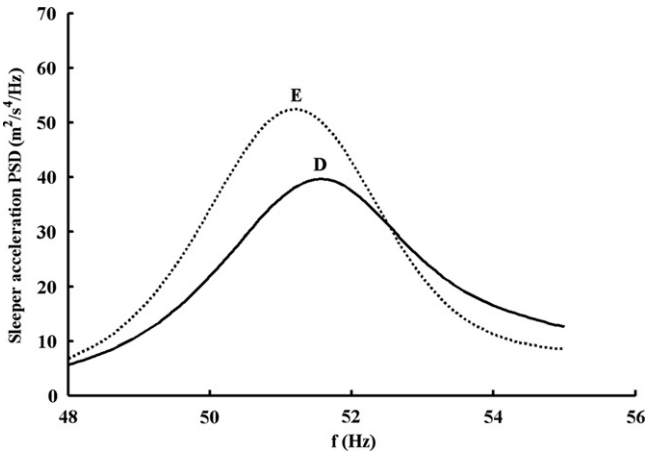

Fig. 6. PSD of sleeper vertical acceleration.

the fixed-vehicle model and 1.5451×10^7 N^2/Hz for the moving-vehicle model, a difference in excess of 100%. In addition, it is found that with increasing vehicle velocity, the difference between the results calculated by the two models also increases.

Fig. 6 gives the vertical acceleration PSD curves of the sleeper under the 1st wheelset. Only the results between frequencies 48–55 Hz are shown, to make the peaks clear. It can be seen that the results calculated by the two models are quite different. The peak value for the fixed-vehicle model at point D is 39.5725 m^2/s^4/Hz and for the moving-vehicle model at point E is 52.4057 m^2/s^4/Hz. The error is 24.49% and the peaks correspond to different frequencies. Similar conclusions can also be drawn by comparing the PSDs of the rail and the ballast. Figs. 4–6 lead to the following conclusions: Since the global dynamic responses of the vehicle body and bogies are nearly zero-mean and stationary, the results calculated by the fixed-vehicle model are also reliable. On the other hand, the local non-zero-mean dynamic responses of the wheel–track system are only reliable when they are calculated by the moving-vehicle model.

6.3. *Influence of vehicle velocity*

Vehicle velocity has an important influence on system responses. Fig. 7 gives the response PSD curves of the vehicle at velocities of 80, 160 and 250 km/h. As shown in Fig. 7(a), when v=80 km/h, the main peak, A, of the body acceleration PSD curve is at about 1.2 Hz. As the velocity is increased to 160 km/h, peak A decreases, while the corresponding frequency increases to about 2.1 Hz. In addition, the smaller peak, B, grows as the frequency increases to about 1 Hz. If the velocity is further increased to 250 km/h, peak B at about 1 Hz increases remarkably and becomes the new main peak, while peak A further decreases and becomes the second highest peak at about 3.2 Hz. This clearly indicates that the peak of the body

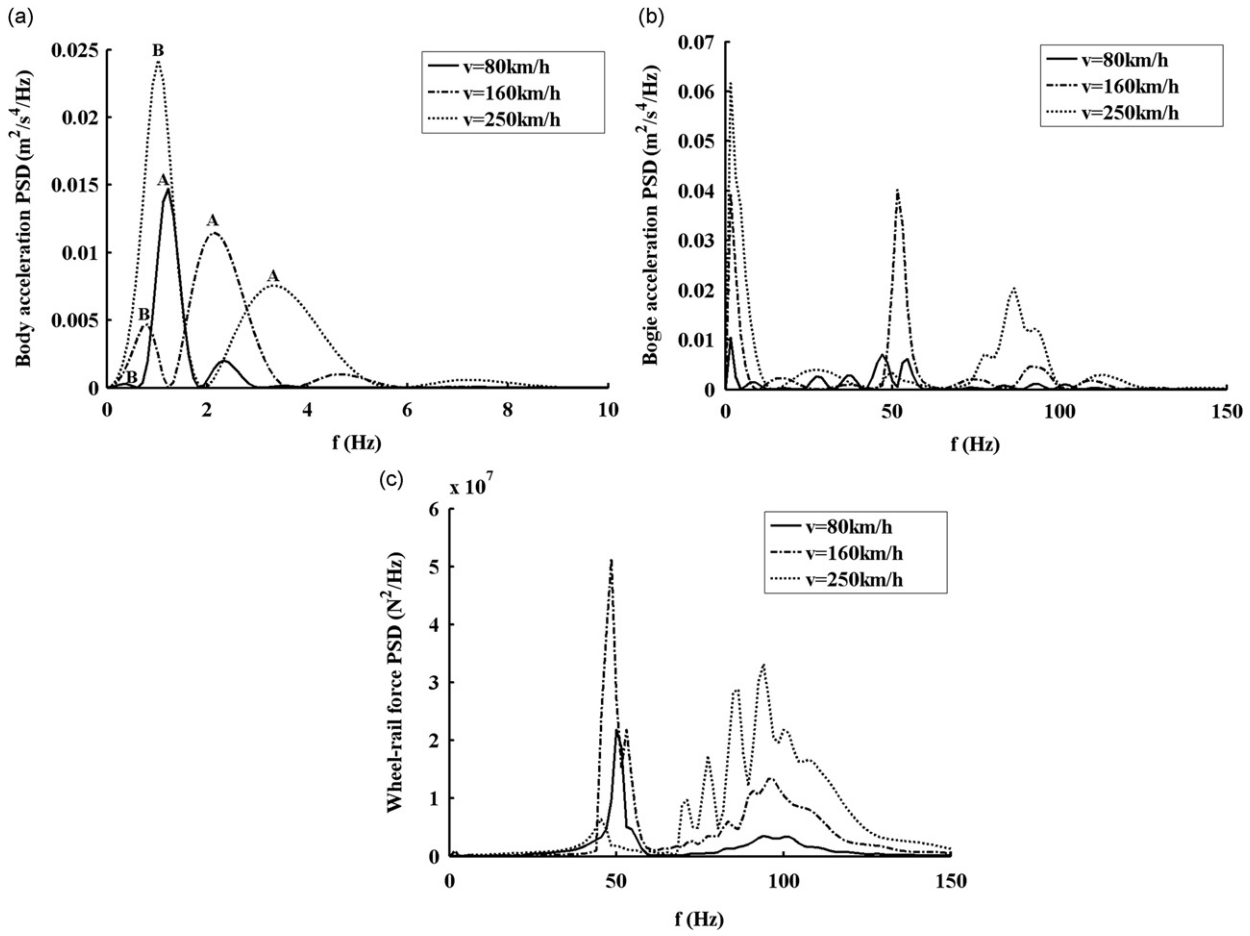

Fig. 7. PSDs of vehicle responses at different velocities: (a) body vertical acceleration, (b) 1st bogie vertical acceleration, and (c) 1st wheel–rail contact force.

acceleration PSD curve does not always increase with the vehicle velocity. In order to establish a picture of how the peaks vary with the vehicle velocity, the body acceleration PSDs at velocities between 80 and 250 km/h were investigated. The results show that with increasing velocity, the peak frequencies at A and B of Fig. 7(a) move towards the right with the peak values decreasing at A and increasing at B. The two peaks coincide with each other at a velocity of about 190 km/h, which agrees with Ref. [3]. In addition, as shown in Fig. 7(b), there exist extra peaks near 50 and 90 Hz on the bogie acceleration PSD curve. Comparing Fig. 7(a–c), it is clear that the peaks at several frequencies can be attributed to the influence of body response, while the peaks at 50 and 90 Hz are attributable to the influence of the wheel–rail force. Usually, such peaks would appear near the natural frequencies of the system. For the moving-vehicle model, however, the distribution of load PSD in the frequency domain considerably affects the PSDs of responses. In turn, the responses caused by different loads will superpose or counteract in different ways, depending heavily on the vehicle velocity. This leads to the complex phenomena shown across Fig. 7(a–c).

Fig. 8 gives the response PSD curves of the rail, sleeper and ballast under the 1st wheel pair at different velocities. It can be seen that although the peaks at several frequencies appear on all the PSD curves, they have very little effect on the responses of the track system, due to the low-frequency components of the interactive forces. The vibration energy of the rail and the sleepers is concentrated in a frequency band from tens to thousands of Hz while the equivalent band for ballast stretches across tens to a hundred of Hz. As the velocity increases, the responses increase as well; however, the vibration energy distribution with frequency does not vary significantly.

6.4. *Influences of class of track*

The class of track is also a very important factor in the responses of the coupled system. In this section, responses at a velocity of 200 km/h for classes 4–6 track are discussed.

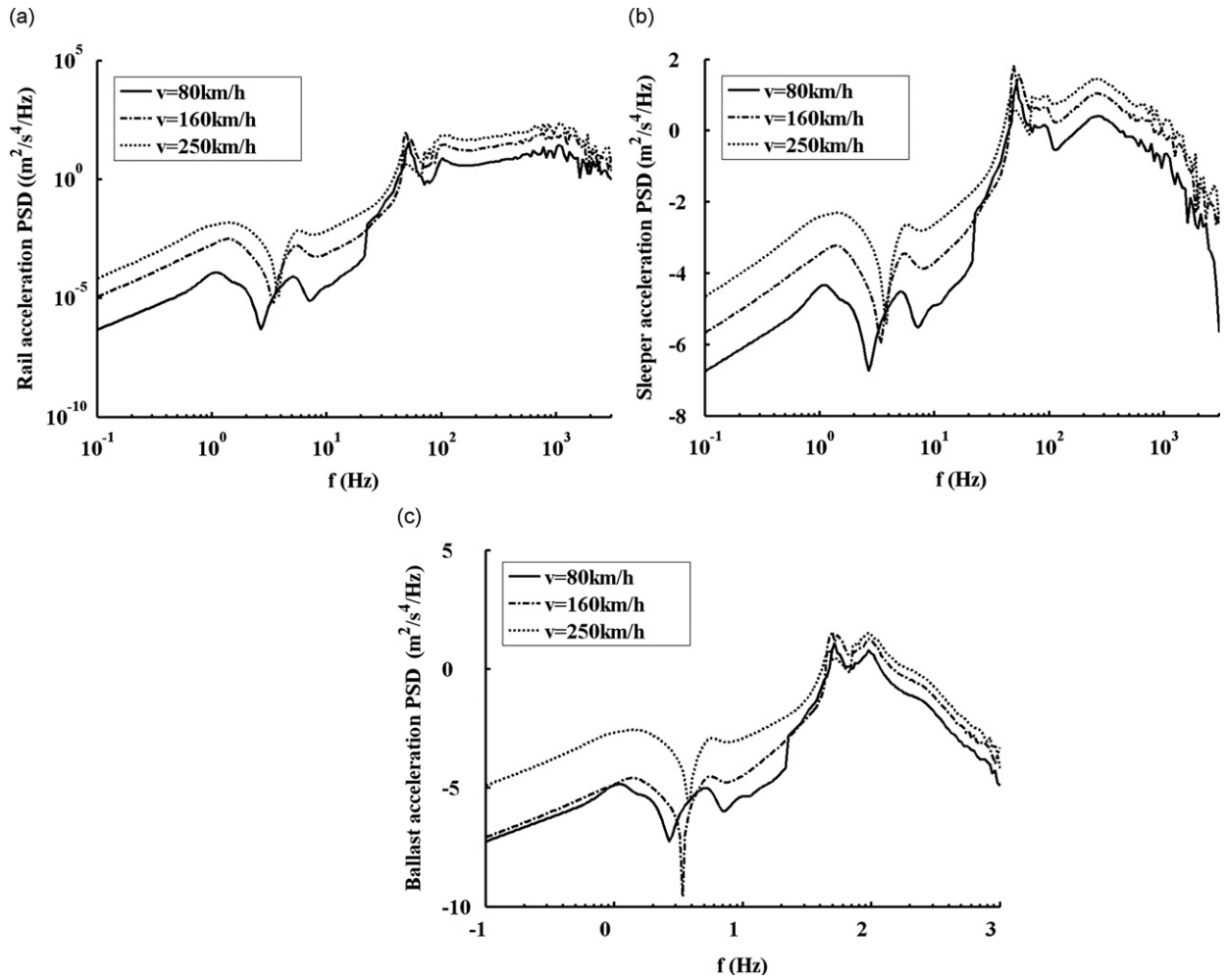

Fig. 8. PSD of track vertical accelerations at different velocities: (a) rail, (b) sleeper, and (c) ballast.

As shown in Fig. 9(a), the class of track has a great influence on the responses of the vehicle. The lower the class of track is, the stronger the responses of the vehicle are, but the distribution of vibration energy in the frequency domain varies very little.

Fig. 9(b)–(d) give the PSDs of rail, sleeper and ballast under the 1st wheel pair for different classes of track. It can be seen that the class of track only affects the dynamic responses of the track structure significantly when the frequency is lower than 100 Hz and has almost no effect when the frequency is higher than 100 Hz. It is clear that the high-frequency responses of the track are caused by the track itself and therefore have little relation to the class of track.

7. Conclusions

An innovative method has been proposed that combines the pseudo-excitation method, symplectic mathematical scheme and Schur decomposition scheme to analyze the random responses of coupled vehicle–track systems. The method is justified by comparison with a very much slower Monte-Carlo simulation. The following general conclusions can be drawn from the paper.

1. The dynamic responses of the vehicle body and bogies are nearly zero-mean and stationary, so that the results obtained using a fixed-vehicle model are also reliable. However, this is not so when computing responses of the wheels and track system, which must be calculated by the moving-vehicle model.
2. Vehicle velocity has an important influence on system responses. As the vehicle velocity increases, the responses of vehicle do not always follow suit. However, while the responses of track increase with velocity, the distribution of track vibration energy in the frequency domain varies very little.

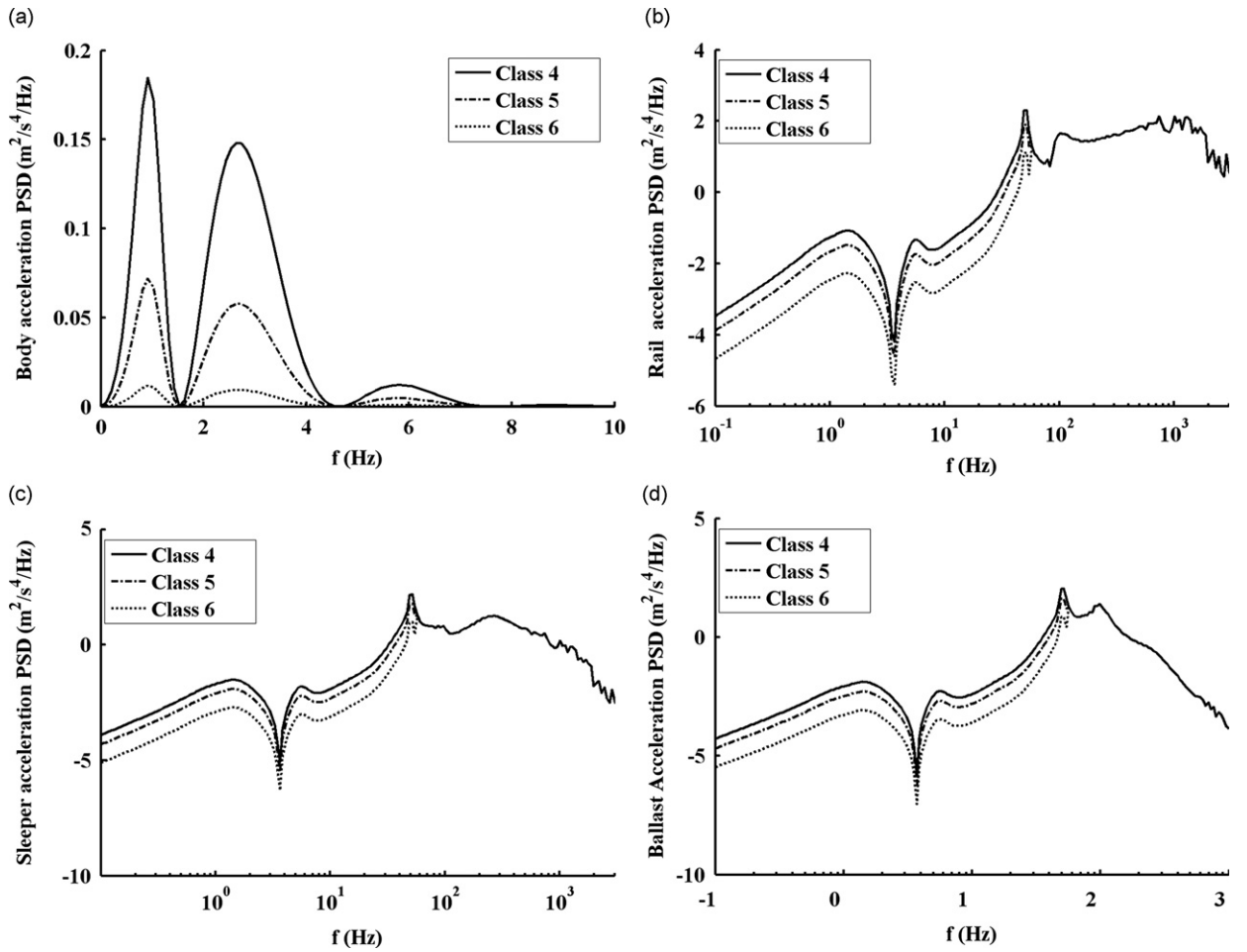

Fig. 9. PSD of vertical accelerations for different classes of track for a vehicle traveling at 200 km/h: (a) vehicle body, (b) rail, (c) sleeper, and (d) ballast.

3. The class of track has a great influence on the responses of the vehicle, but has rather little influence on the responses of the track itself, especially in the high-frequency regions, where the influence can be ignored completely.

The symplectic method presented in the paper was used to reduce the dof of the track. It can also be used to derive responses of periodic structures subject to arbitrary loads, or be extended to other fields, such as optimization or control of coupled vehicle–track systems. Although only one carriage was considered in the numerical examples, a train with any number of locomotives and carriages can be dealt with similarly.

Acknowledgements

Support for this work from the National Natural Science Foundation of China (nos. 10972048, 90815023, 50608012, and 10972048), the National 973 Plan Project (no. 2010CB832700) and the Cardiff Advanced Chinese Engineering Centre are gratefully acknowledged.

References

[1] G. Chen, The Analysis on Random Vibration of Vehicle/track Coupling System, PhD Thesis, Southwest Jiaotong University, 2000 (in Chinese).
[2] C.H. Li, G.F. Wan, Random vibration of track structure, *Journal of the China Railway Society* 20 (1998) 97–101 (in Chinese).
[3] F. Lu, D. Kennedy, F.W. Williams, J.H. Lin, Symplectic analysis of vertical random vibration for coupled vehicle–track systems, *Journal of Sound and Vibration* 317 (2008) 236–249.
[4] J. Xu, C.R. Jiang, W.P. Xie, Research on track structure of Wuhan light rail based on the random vibration theory, *Journal of Wuhan University of Technology* 29 (2007) 100–103 (in Chinese).
[5] X. Lei, N.A. Noda, Analyses of dynamic response of vehicle and track coupling system with random irregularity of track vertical profile, *Journal of Sound and Vibration* 258 (2002) 147–165.

[6] K.Y. Wang, J.X. Liu, W.M. Zhai, C.B. Cai, Simulation on safety and comfort of a moving train, *Journal of Traffic and Transportation Engineering* 6 (2006) 9–12 (in Chinese).
[7] J. Shi, Q.C. Wei, C.F. Wan, Y.S. Deng, Study on dynamic responses of high-speed maglev vehicle/guideway coupling system under random irregularity, *Chinese Journal of Theoretical and Applied Mechanics* 38 (2006) 850–857 (in Chinese).
[8] X.Y. Long, Q.C. Wei, Y.W. Feng, J. Shi, Dynamic response of linear metro vehicle/track excited by track irregularity, *Journal of Traffic and Transportation Engineering* 8 (2008) 9–13 (in Chinese).
[9] J.H. Lin, Y.H. Zhang, in: *Pseudo Excitation Method in Random Vibration*, Science Press, Beijing, 2004 (in Chinese).
[10] J.H. Lin, Y.H. Zhang, in: *Vibration and Shock Handbook, Seismic Random Vibration of Long-span Structures*, CRC Press, Boca Raton, FL, 2005 (Chapter 30).
[11] F. Lu, Q. Gao, J.H. Lin, F.W. Williams, Non-stationary random ground vibration due to loads moving along a railway track, *Journal of Sound and Vibration* 298 (2006) 30–42.
[12] L. Gry, C. Gontier, Dynamic modelling of railway track: a periodic model based on a generalized beam formulation, *Journal of Sound and Vibration* 199 (1997) 531–558.
[13] D.J. Thompson, Vehicle–rail noise generation, part 3: rail vibration, *Journal of Sound and Vibration* 161 (1993) 421–446.
[14] H. Kruse, K. Popp, T. Krzyzynski, On steady state dynamics of railway tracks modeled as continuous periodic structures, *Machine Dynamics Problems* 20 (1998) 149–166.
[15] Y.K. Lin, T.J. McDaniel, Dynamics of beam type periodic structures, *Journal of Engineering for Industry* 91 (1969) 1133–1141.
[16] D.J. Mead, A general theory of harmonic wave propagation in linear periodic systems with multiple coupling, *Journal of Sound and Vibration* 27 (1973) 235–260.
[17] D.J. Mead, Wave propagation and natural modes in periodic systems: I. Mono-coupled systems. II. Multi-coupled systems, with and without damping, *Journal of Sound and Vibration* 40 (1–18) (1975) 19–39.
[18] D.W. Miller, A.H. Von Flotow, A travelling wave approach to power flow in structural networks, *Journal of Sound and Vibration* 128 (1989) 145–162.
[19] Y. Yong, Y.K. Lin, Propagation of decaying waves in periodic and piecewise periodic structures of finite length, *Journal of Sound and Vibration* 129 (1989) 99–118.
[20] F.W. Williams, W.X. Zhong, P.N. Bennett, Computation of the eigenvalues of wave propagation in periodic sub-structural systems, *Journal of Vibration and Acoustics* 115 (1993) 422–426.
[21] W.X. Zhong, F.W. Williams, Wave problems for repetitive structures and symplectic mathematics, *Proceedings of the Institution of Mechanical Engineers, Part C* 206 (1992) 371–379.
[22] W.X. Zhong, F.W. Williams, The eigensolutions of wave propagation for repetitive structures, *International Journal of Structural Engineering and Mechanics* 1 (1993) 47–60.
[23] J.H. Lin, Y. Fan, P.N. Bennett, F.W. Williams, Propagation of stationary random waves along substructural chains, *Journal of Sound and Vibration* 180 (1995) 757–767.
[24] J.H. Lin, Y. Fan, F.W. Williams, Propagation of non-stationary waves along substructural chains, *Journal of Sound and Vibration* 187 (1995) 585–593.
[25] H. Amann, G. Metzen, in: *Ordinary Differential Equations: An Introduction to Nonlinear Analysis (Gerhard Metzen, trans.)*, Walter de Gruyter, Berlin, 1990.
[26] D.E. Newland, in: *An Introduction to Random Vibrations and Spectral Analysis*, Longman, London, 1975.
[27] Y.B. Yang, Y.S. Wu, A versatile element for analyzing vehicle–bridge interaction response, *Engineering Structures* 23 (2001) 452–467.